Eric A. Müller
Florian Kolb
Lino Guzzella

Department of Mechanical and Process Engineering,
ETH Zurich,
8092, Zurich, Switzerland

Anna G. Stefanopoulou[1]
e-mail: annastef@umich.edu

Denise A. McKay

Department of Mechanical Engineering,
University of Michigan,
Ann Arbor, MI 48109

Correlating Nitrogen Accumulation With Temporal Fuel Cell Performance

The permeability or crossover characteristics of a typical perfluorosulfonic acid base type membrane are used for the temporal and spatial estimations of nitrogen concentration along the anode channels of a polymer electrolyte membrane fuel cell stack. The predicted nitrogen accumulation is then used to estimate the impact of local fuel starvation on stack voltage through the notion of apparent current density. Despite the simplifying assumptions on the water accumulation and membrane hydration levels, the calibrated model predicts reasonably well the response of a 20-cell stack with a dead-ended anode. Specifically, the predicted voltage decay and the estimated gas composition at the anode outlet are experimentally validated using the stack-averaged voltage and a mass spectrometer. This work shows that the crossover of nitrogen and its accumulation in the anode can cause a considerable decay in stack voltage and should be taken into account under high hydrogen utilization conditions. [DOI: 10.1115/1.3177447]

1 Introduction

Fuel cells fed with compressed and high-purity hydrogen can, in principle, operate dead-ended with very high hydrogen utilization eliminating the need to recuperate the energy lost due to the hydrogen that exits the stack unused [1,2]. The associated high fuel efficiency and low-hardware complexity cannot always be realized because frequent anode purging (short duration event of high hydrogen flow) is necessary to remove the nitrogen and water that cross from the cathode to the anode through the fuel cell membrane. The accumulation of inert gas in the anode can restrict reactant transport, and consequently, cause cell voltage degradation. The cell performance can be restored by purging the inert gas although severe blocking can cause irreversible degradation [3].

In dead-ended stacks, purging is typically scheduled using fixed time intervals or charge intervals (based on amp hours). These purge schedules rely on extensive testing and include very high safety factors to account for uncertainties. High safety factors translate to frequent purging, which, in turn, decrease fuel efficiency. As a result validated models of water and nitrogen accumulation in the anode will facilitate the development of optimum and safe purge schedules based on model-based control techniques. The robustness of these purge schedules can be enhanced by taking into account the measured cell voltage to provide valuable feedback of the actual inert gas accumulation in the cell. The integration of the voltage measurement as a feedback relies also on the availability of a model that predicts the voltage degradation associated with inert gas accumulation. Specifically, the estimated voltage is compared with the actual voltage and the error is used to adjust the model-based purge schedule. A similar model-based technique was used for the estimation of hydrogen starvation [4] and control of the hydrogen production rate from a fuel processor [5].

To facilitate such a model-based control design for dead-ended anode fuel cell stacks, we developed a model that predicts the nitrogen accumulation along the channels of a fuel cell stack and the associated voltage degradation. Note that in this work, the accumulation of water in the anode is neglected but it is separately pursued in Ref. [6]. Here, the nitrogen accumulation along the channels is quantified in an effort to distinguish the effects of these two distinct transport mechanisms (nitrogen versus water) on fuel cell voltage degradation. The estimation of the temporal and spatial nitrogen concentrations is based on permeability coefficients from Ref. [7]. The one-dimensional model in Ref. [7] offered insight on how hydrogen utilization and anode recirculation affects the steady-state nitrogen accumulation along the channel. Our model extends the previous steady-state cell model by including (i) temporal effects, (ii) prediction of voltage degradation, and (iii) validation with stack measurements.

The gas composition along the anode flow channels is estimated and experimentally validated by continuously sampling the stack outlet manifold gases with a mass spectrometer. The modeled nitrogen accumulation along the channels causes local fuel starvation, which is used to predict the temporal and stack-average voltages by utilizing the notion of apparent current density. The apparent current density originally used in Ref. [6] and later in Ref. [8] to capture the effect of the fuel cell area blocked by water accumulation is a simplification of the spatially distributed phenomenon of local starvation and approximates the increase in current density due to the fuel cell area blocked by nitrogen.

The effect of local fuel starvation on voltage is typically modeled by coupling the Butler–Volmer overpotential with the associated local current density integrated along the channel [9–11]. Although this multidimensional modeling approach is more representative of what physically happens in an operating fuel cell, it is difficult to numerically implement, calibrate, and validate with large stacks under dynamically changing conditions [12]. Apart from multidimensional models using complex partial differential equations (PDEs), simple zero-dimensional models using homogeneous channel pressure and concentration cannot capture the effects of the nitrogen crossover and accumulation in the anode. Indeed, the maximum nitrogen accumulation that can be predicted with a zero-dimensional model will be the nitrogen concentration in a cathode channel, which is not great enough to cause the experimentally observed decrease in cell voltage.

This modeling work attempts to balance the tradeoff between modeling complexity and accuracy by combining an along-the-channel one-dimensional PDE model with calculations of the apparent active channel length and hence the apparent current density. Section 2 discusses the experimental setup and stack measurements. Section 3 details the formulation of the partial dif-

[1]Corresponding author.

Manuscript received April 6, 2008; final manuscript received December 27, 2008; published online January 12, 2010. Review conducted by Abel Hernandez. Paper presented at the 2008 Dynamic Systems and Controls Conference (DSC2008), Ann Arbor, MI, October 20–22, 2008.

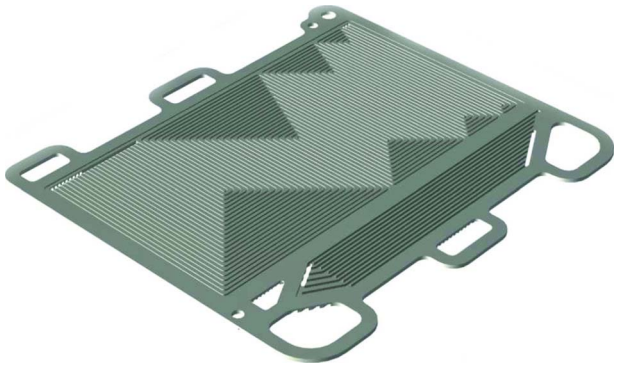

Fig. 1 Anode flow field (source: Paul Scherrer Institute (PSI))

ferential equations along with their initial and boundary conditions, the discretization approach for the numerical solution, the model of the gas concentrations at the stack outlet manifold and the voltage response. Then, simulations are used to investigate the prediction sensitivity associated with two important variables. The simulation results, together with the comparisons against experimental data, are also shown.

Simulations show that the predicted voltage captures accurately the observed voltage decay (6 mV/min) but underpredicts the duration of the initial flat voltage response. Moreover, the predicted voltage reaches an equilibrium value after 1250 s but the measured voltage keeps on dropping after 1250 s. We postulate that our simple cell-average model based on apparent current density is not valid when a large percentage of the active area is covered with a blanket of inert gas because the experimental data show increased cell-to-cell variations. Finally, the model reaches steady state outlet concentrations within 600 s, which matches the actual concentration measurements.

2 Experimental Setup

Through a joint venture with ETH Zurich and other academic and industrial partners, a hybrid fuel cell vehicle, named the PAC-Car, was designed and constructed to examine the fuel efficiency limits of road vehicles. A fuel cell stack from the PAC-Car [13] was installed on a test bench and used to generate all the experimental data presented in this work. The stack uses Umicore H200 membranes, which are Nafion®-type 112 membranes with a platinum load of 0.6 mPt/cm^2. The gas diffusion layers are Toray™ 090 with 80% porosity before compression. These materials allow us to use similar permeability coefficients with the ones identified in Ref. [7].

The flow field on the anode side was designed to maintain approximately constant gas speed and pressure along the channels. As a result, the number of channels is sequentially reduced from 24 channels in parallel at the inlet to 3 channels at the outlet as shown in Fig. 1. This special channel configuration is taken into account in the modeling approach via appropriate boundary conditions.

Internal humidifiers were used to humidify the anode and cathode inlet flows [14]. An air mass flow controller maintains the desired air excess ratio, which is the flow supplied in excess to the flow necessary for the stoichiometric reaction associated with the current drawn. Pressure regulators control the anode and cathode gauge pressures. The coolant outlet temperature was thermostatically controlled to a desired value with an on-off controlled fan. A solenoid valve at the anode outlet allows anode purging. The hydrogen and nitrogen concentrations are measured using a fast mass spectrometer (Omni Star, GSD 301 C1 by Pfeiffer Vacuum, Nashua NH 03063). The mass spectrometer continuously samples a small stream from the anode and determines the composition of the gas flow. The flow to the mass spectrometer is a very small

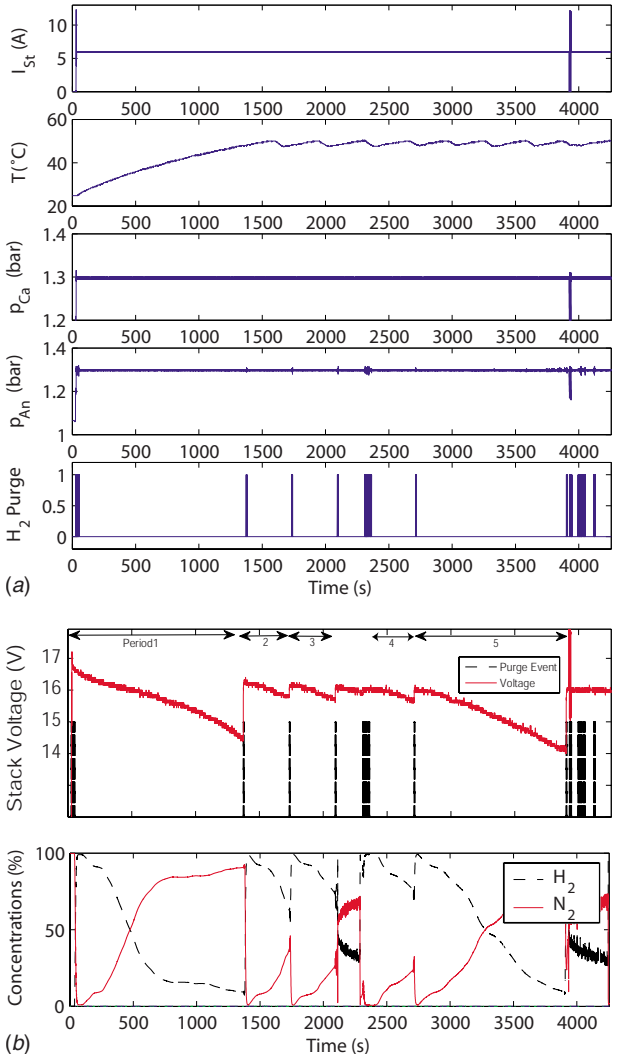

Fig. 2 Experimental data show the operating conditions in the first four subplots in (*a*) with the output signals shown in the last two subplots in (*b*)

fraction of the hydrogen mass flow rate necessary for the reaction, and hence the experimental conditions are exemplary of stack operation with a dead-ended anode.

Figure 2(*a*) shows a representative set of experimental data from the stack. After the initial stack warm-up period, which lasts 1500 s, the stack operates at 50 °C under constant load (6 A) and constant anode and cathode pressures. The air flow controller is set to provide twice the air flow needed for stoichiometric reaction (λ_{air}=200%). The measured stack voltage and the measured hydrogen and nitrogen gas concentrations at the anode outlet are shown in Fig. 2(*b*). As can be seen, the concentration of nitrogen increases after each purge. Several purges are initiated to verify that the voltage and concentrations in between purges are repeatable. Multiple purges at the 2300th second and 3900th second are initiated to remove the high water concentration, which causes the observed oscillation in the measured concentration signals. Various purge events define different periods, which are folded in time later on to facilitate model validation. Due to the warm-up phase and to the high water concentration this particular set of data is not best for model validation but it highlights some of the intricate aspects of the experiment, and hence, provide a good background to the reader before the technicalities of the model development are presented. Note that for model validation, higher temperature

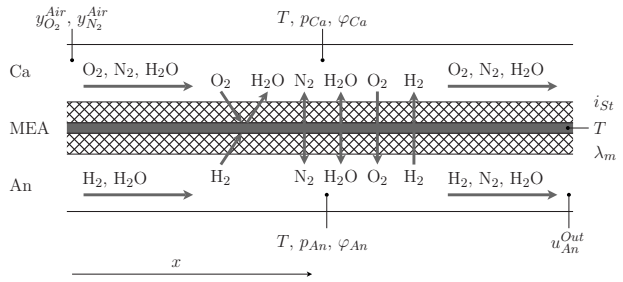

Fig. 3 Diagram of constituent mass transport and flows within the fuel cell

(60°C instead of 50°C) and higher air excess ratio (290% instead of 200%) are later used to reduce the water accumulation in the anode.

3 Mathematical Model

The model of the anode flow field is based on the equations of mass conservation. The gas concentrations in the anode channels of a fuel cell system are determined from the properties of the gas streams entering and leaving the channels through the inlet and outlet orifices by knowing the production or consumption of gas constituents due to chemical reactions and by knowing the cross-over of gases across the fuel cell membrane. Diffusion is neglected and a constant flow out of the anode channel is employed for the calculation of the convective flow. The crossover of gases across the membrane is determined by the permeability coefficients of the membrane and the membrane thickness [7]. In Fig. 3, a schematic of the membrane electrode assembly (MEA) sandwiched between the gas diffusion layers and the anode and cathode channels ("An" and "Ca," respectively) is shown, indicating the constituent transfer through the membrane as well as the inlet and outlet mass flow rates.

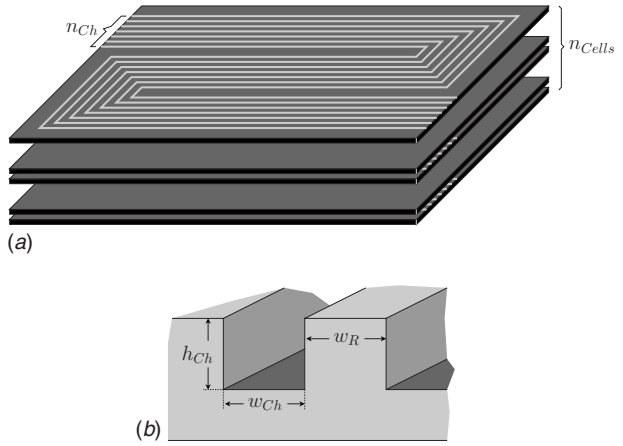

Fig. 4 A (*a*) generic anode flow field and (*b*) anode geometry

Important inputs to the system are the stack current I_{St}, the temperature of the system T, the anode pressure p_{An}, the cathode pressure p_{Ca}, and the anode and cathode relative humidities φ_{An} and φ_{Ca}.

Other important properties of the system are determined by the system's geometry. Relevant geometrical parameters, as shown in Fig. 4(*a*), are the number of fuel cells in the stack n_{Cells} and the number of parallel channels in the anode flow field n_{Ch}. Other geometrical parameters such as the width w_{Ch}, the height h_{Ch} and the length L_{Ch} of an anode channel, and the width between two adjacent channels w_R are shown in Fig. 4(*b*). The particular values for the PAC-Car's fuel cell system are summarized in Table 1 in the Appendix.

First, few preliminary definitions and assumptions are introduced. Then, the mass conservation laws are formulated. The source terms emerging in the conservation equations are detailed and the initial and the boundary conditions are defined. A method to discretize the model equations is shown next. The outlet manifold dynamics and the corresponding nitrogen concentration in the anode outlet manifold are modeled and compared with the mass spectrometer measurements that are collected in the anode outlet manifold of the stack. Finally the nitrogen accumulation in the cell channel is used to scale the cell area available for reaction, called the apparent cell area, which is subsequently used to predict the stack voltage response.

3.1 Preliminaries. The gas mixtures in the anode channels and the cathode channels are described as mixtures of ideal gases and are assumed to obey Dalton's law where the pressure of an ideal gas mixture is equal to the sum of the partial pressures of its components,

Table 1 Parameters of the system

Parameter	Symbol	Value
Geometry		
No. of fuel cells	n_{Cells}	20
No. of parallel channels in the anode flow field	n_{Ch}	(24,12,6,3)
Length of the stages in the anode flow field	L_{Ch}	(0.19,0.17,0.16,0.15) m
Width of an anode channel	w_{Ch}	0.8×10^{-3} m
Height of an anode channel	h_{Ch}	0.35×10^{-3} m
Rib width of the anode flow field	w_R	0.9×10^{-3} m
Membrane thickness	δ	50×10^{-6} m
Cell active area	A_{Active}	136×10^{-4} m^2
Cross-sectional area of anode outlet manifold	A_{MF}	11×10^{-6} m^2
Length of anode outlet manifold	L_{MF}	79×10^{-3} m
Gas crossover		
First permeability coefficient for hydrogen permeation	$\kappa_1^{H_2}$	6.6×10^{-11} mol m^{-1} s^{-1} Pa^{-1}
Second permeability coefficient for hydrogen permeation	$\kappa_2^{H_2}$	21.03×10^3 J mol^{-1}
First permeability coefficient for oxygen permeation	$\kappa_1^{O_2}$	$0.5\cdot\kappa_1^{H_2}$
Second permeability coefficient for oxygen permeation	$\kappa_2^{O_2}$	$\kappa_2^{H_2}$
Permeation coefficient of N_2	k_{N_2}	1.0×10^{-14} mol m^{-1} s^{-1} Pa^{-1}

$$p = \sum_i p_i = \sum_i y_i p \tag{1}$$

where y_i is the molar fraction of species i. Combined with the ideal gas law $p_i V = m_i R_i T$ the individual component mass is computed.

$$m_i = \frac{p_i V}{(R/M_i)T} = y_i \frac{pV}{(R/M_i)T} \tag{2}$$

In order to keep the programming effort low, the conditions on the cathode side are assumed constant.

$$\begin{aligned} p_{\mathrm{Ca}}(x,t) &\equiv p_{\mathrm{Ca}}, \quad \varphi_{\mathrm{Ca}}(x,t) \equiv \varphi_{\mathrm{Ca}} \\ y_{\mathrm{O_2}}^{\mathrm{Air}}(x,t) &\equiv y_{\mathrm{O_2}}^{\mathrm{Air}}, \quad y_{\mathrm{N_2}}^{\mathrm{Air}}(x,t) \equiv y_{\mathrm{N_2}}^{\mathrm{Air}} \end{aligned} \tag{3}$$

implying constant cathode partial pressures for oxygen, nitrogen, and vapor. If, furthermore, anode temperature T and total pressure p_{An} are assumed to be constant over time and space,

$$T(x,t) \equiv T, \quad p_{\mathrm{An}}(x,t) \equiv p_{\mathrm{An}} \tag{4}$$

the anode mass balance equation can be formulated in terms of molar fractions. The water content of the membrane and the anode relative humidity are assumed to be constant as well.

$$\lambda_m(t) \equiv \lambda_m, \quad \varphi_{\mathrm{An}}(x,t) \equiv \varphi_{\mathrm{An}} \tag{5}$$

Note that in practice, the membrane water content and the anode relative humidity are functions of many operating variables, such as temperature, stack current, and cathode relative humidity. In this model the spatial and temporal variations in the membrane water content and their effects on membrane crossover and voltage performance have been neglected. Here, the membrane water content and the anode relative humidity are assigned constant values in an effort to clarify the relative contributions of the nitrogen and water accumulation to voltage decay.

3.2 Mass Conservation Equations for the Anode. A mass balance on a control volume in an anode channel yields a PDE for the mass of each component $i \in \{\mathrm{H_2}, \mathrm{N_2}, \mathrm{H_2O}\}$ of the gas stream traveling with velocity $u(x,t)$.

$$\frac{d}{dt} m_i^{\mathrm{An}}(x,t) = -\frac{\partial}{\partial x}[u(x,t) m_i^{\mathrm{An}}(x,t)] + \dot{m}_i^{\mathrm{An}}(x,t) \tag{6}$$

Equation (6) is a convection equation with an additional source term. By substituting Eq. (2) into Eq. (6) and applying assumption (4), the convection equation (6) can be written with respect to molar fractions $y_i^{\mathrm{An}}(x,t)$ as follows:

$$\frac{d}{dt} y_i^{\mathrm{An}}(x,t) = -\frac{\partial}{\partial x}[u(x,t) y_i^{\mathrm{An}}(x,t)] + \dot{y}_i^{\mathrm{An}}(x,t) \tag{7}$$

Since the molar fractions of a gas mixture sum to one ($\Sigma_i y_i^{\mathrm{An}}(x,t) = 1$), the mass balance for the gas mixture yields

$$\sum_i \frac{d}{dt} y_i^{\mathrm{An}}(x,t) = -\sum_i \frac{\partial}{\partial x}[u(x,t) y_i^{\mathrm{An}}(x,t)] + \sum_i \dot{y}_i^{\mathrm{An}}(x,t) = 0 \tag{8}$$

While the conservation equation (7) describes the variation in the molar fractions of the gas mixture over time and along the channels, the overall balance (8) can be used to determine the flow speed of the gas mixture.

3.3 Production/Consumption Rates. The source terms $\dot{y}_i^{\mathrm{An}}(x,t)$ in Eqs. (7) and (8) reflect the component production/consumption rates. In the following, these rates are quantified for each component based on prior work in Ref. [7].

3.3.1 Hydrogen. The consumption rate of hydrogen (in $\mathrm{s^{-1}}$) can be expressed as

$$\dot{y}_{\mathrm{H_2}}^{\mathrm{An}}(x,t) = -\frac{RT}{p_{\mathrm{An}}} \cdot \frac{w_{\mathrm{Ch}} + w_R}{w_{\mathrm{Ch}} h_{\mathrm{Ch}}} \cdot \left(\frac{k_{\mathrm{H_2}}}{\delta} y_{\mathrm{H_2}}^{\mathrm{An}}(x,t) p_{\mathrm{An}} + 2\frac{k_{\mathrm{O_2}}}{\delta} p_{\mathrm{O_2}}^{\mathrm{Ca}} + \frac{1}{2F} i_{\mathrm{St}}^{\mathrm{App}}(t) \right) \tag{9}$$

The consumption rate (9) is valid only when and where hydrogen is available, i.e., when $y_{\mathrm{H_2}}^{\mathrm{An}}(x,t) > 0$. For the numerical implementation, we select a small positive value $y_{\mathrm{H_2}}^{\mathrm{AnStarv}} = 0.001$ instead of zero to define the onset of hydrogen starvation where the hydrogen consumption is set to zero.

$$\dot{y}_{\mathrm{H_2}}^{\mathrm{An}}(x,t) = 0 \quad \text{if} \quad y_{\mathrm{H_2}}^{\mathrm{An}}(x,t) < y_{\mathrm{H_2}}^{\mathrm{AnStarv}} \tag{10}$$

In Eq. (9), the first term in the parenthesis describes the losses of hydrogen due to the crossover flow to the cathode side. The permeation rate is assumed to be proportional to the difference in partial pressures across the membrane and the permeability coefficient and is inversely proportional to the membrane thickness. The second term in the parenthesis describes the consumption of hydrogen due to the permeation of oxygen across the membrane from the cathode.[2] The third term in the parenthesis describes the consumption of hydrogen due to the electrochemical reaction, which is proportional to the apparent current density $i_{\mathrm{St}}^{\mathrm{App}}(t)$. The apparent current density considers the reduction in active fuel cell area due to local fuel starvation.

$$i_{\mathrm{St}}^{\mathrm{App}}(t) = \frac{I_{\mathrm{St}}}{A_{\mathrm{Active}}^{\mathrm{App}}(t)} \tag{11}$$

with apparent active area

$$A_{\mathrm{Active}}^{\mathrm{App}}(t) = n_{\mathrm{Ch}}(w_{\mathrm{Ch}} + w_R) L_{\mathrm{App}}(t) \tag{12}$$

based on the channel length

$$L_{\mathrm{App}}(t) = \{x | y_{\mathrm{H_2}}^{\mathrm{An}}(x,t) > y_{\mathrm{H_2}}^{\mathrm{AnStarv}}\} \tag{13}$$

The partial pressure of oxygen in the cathode $p_{\mathrm{O_2}}^{\mathrm{Ca}}$ is calculated as

$$p_{\mathrm{O_2}}^{\mathrm{Ca}} = y_{\mathrm{O_2}}^{\mathrm{Air}}(p_{\mathrm{Ca}} - \varphi_{\mathrm{Ca}} p_{\mathrm{Sat}}(T)) \tag{14}$$

where $p_{\mathrm{Sat}}(T)$ is the vapor saturation pressure at temperature T. The permeation coefficients of hydrogen and oxygen are modeled according to Ref. [7] as

$$k_{\mathrm{H_2}} = \kappa_1^{\mathrm{H_2}} \exp\left(-\frac{\kappa_2^{\mathrm{H_2}}}{RT}\right) \tag{15}$$

$$k_{\mathrm{O_2}} = \kappa_1^{\mathrm{O_2}} \exp\left(-\frac{\kappa_2^{\mathrm{O_2}}}{RT}\right) \tag{16}$$

where the change in the permeability coefficients with membrane hydration is neglected.

3.3.2 Nitrogen. The crossover of nitrogen due to concentration gradients is expressed as

$$\dot{y}_{\mathrm{N_2}}(x,t) = \frac{RT}{p_{\mathrm{An}}} \cdot \frac{w_{\mathrm{Ch}} + w_R}{w_{\mathrm{Ch}} h_{\mathrm{Ch}}} \cdot \frac{k_{\mathrm{N_2}}}{\delta} (p_{\mathrm{N_2}}^{\mathrm{Ca}} - y_{\mathrm{N_2}}^{\mathrm{An}}(x,t) p_{\mathrm{An}}) \tag{17}$$

where the partial pressure of nitrogen in the cathode $p_{\mathrm{N_2}}^{\mathrm{Ca}}$ is given as

$$p_{\mathrm{N_2}}^{\mathrm{Ca}} = y_{\mathrm{N_2}}^{\mathrm{Air}}(p_{\mathrm{Ca}} - \varphi_{\mathrm{Ca}} p_{\mathrm{Sat}}(T)) \tag{18}$$

The permeation coefficient of nitrogen $k_{\mathrm{N_2}}$ is assumed to be constant.

3.3.3 Water Vapor. The physical reasons for the production or consumption of vapor are the condensation and evaporation of

[2] Since per molecule of oxygen two molecules of hydrogen are consumed, a factor of 2 is employed. However, in Ref. [7], a factor of 1/2 was proposed.

water inside the anode channels and the transport of vapor across the membrane due to diffusion and electro-osmotic drag. From assumption (5) and the conservation equation (7), the production/consumption rate of water vapor follows as

$$\dot{y}^{\mathrm{An}}_{\mathrm{H_2O}}(x,t) = y^{\mathrm{An}}_{\mathrm{H_2O}} \cdot \frac{\partial}{\partial x} u(x,t) \tag{19}$$

with

$$y^{\mathrm{An}}_{\mathrm{H_2O}} = \frac{\varphi_{\mathrm{An}} p_{\mathrm{Sat}}(T)}{p_{\mathrm{An}}} \tag{20}$$

3.4 Initial and Boundary Conditions. In the following, initial conditions and boundary conditions for the PDEs (7) and (8) are defined. Note that the conditions in all channels of the flow fields of the fuel cells are assumed to be equal.

The initial mole fractions of H_2, N_2, and H_2O in the anode channels form the initial conditions for the convection equation (7). The initial mole fractions are defined as the conditions just after a purge event where the fraction of nitrogen in the fuel cell anode channel is assumed to be negligible.

$$y^{\mathrm{An}}_{\mathrm{H_2}}(x,0) = 1 - y^{\mathrm{An}}_{\mathrm{H_2O}}(x,0) - y^{\mathrm{An}}_{\mathrm{N_2}}(x,0) \tag{21a}$$

$$y^{\mathrm{An}}_{\mathrm{N_2}}(x,0) = 0 \tag{21b}$$

$$y^{\mathrm{An}}_{\mathrm{H_2O}}(x,0) = y^{\mathrm{An}}_{\mathrm{H_2O}} \tag{21c}$$

The boundary conditions of the convection in Eqs. (7) and (8) are given by the molar composition of the gas stream at the anode inlet and the flow speed at the anode outlet (Dirichlet conditions).

$$y^{\mathrm{An}}_{\mathrm{H_2}}(0,t) = 1 - y^{\mathrm{An}}_{\mathrm{H_2O}}(0,t) - y^{\mathrm{An}}_{\mathrm{N_2}}(0,t) \tag{22a}$$

$$y^{\mathrm{An}}_{\mathrm{N_2}}(0,t) = 0 \tag{22b}$$

$$y^{\mathrm{An}}_{\mathrm{H_2O}}(0,t) = y^{\mathrm{An}}_{\mathrm{H_2O}} \tag{22c}$$

$$u(L_{\mathrm{Ch}},t) = u^{\mathrm{Out}}_{\mathrm{An}} \tag{22d}$$

Hence the initial and boundary conditions depend on the model input variables φ_{An}, p_{An}, T, and $\dot{V}^{\mathrm{Out}}_{\mathrm{An}}$. The anode outlet flow speed can be calculated from the specified volume flow rate at the anode outlet $\dot{V}^{\mathrm{Out}}_{\mathrm{An}}$ as

$$u^{\mathrm{Out}}_{\mathrm{An}} = \frac{\dot{V}^{\mathrm{Out}}_{\mathrm{An}}}{n_{\mathrm{Cells}} n_{\mathrm{Ch}} w_{\mathrm{Ch}} h_{\mathrm{Ch}}} \tag{23}$$

In the experimental setup investigated here, the volume flow rate at the anode outlet $\dot{V}^{\mathrm{Out}}_{\mathrm{An}}$ is the flow drawn by the mass spectrometer and was estimated based on pressure measurements using an experiment similar to the leak test.

3.5 Discretization of the Model Equations. For the numerical evaluation, the PDEs (7) and (8) are converted to a system of algebraic equations. The most direct means of discretization is provided by replacing the derivatives by equivalent finite difference approximations. If the time derivatives are represented by a forward difference and a backward difference formula is used for the spatial derivatives,[3] the conservation of Eqs. (7) and (8) can be replaced by

$$\frac{y_i^{j,n+1} - y_i^{j,n}}{\Delta t} = -\frac{u^{j,n} y_i^{j,n} - u^{j-1,n} y_i^{j-1,n}}{\Delta x} + \dot{y}_i^{j,n} \tag{24}$$

and

[3]For positive u, this discretization method is generally referred to as *upwind scheme*.

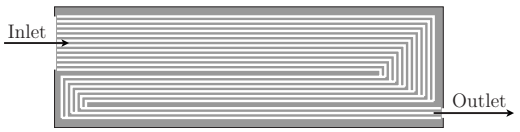

Fig. 5 The employed approximation of PAC-Car II's complex multistage flow field shown in Fig. 1

$$-\sum_i \frac{u^{j,n} y_i^{j,n} - u^{j-1,n} y_i^{j-1,n}}{\Delta x} + \sum_i \dot{y}_i^{j,n} = 0 \tag{25}$$

respectively. Generally, $\xi^{j,n}$ is the value of ξ at the (j,n)th node. The step size Δx is defined by the number of nodes J along an anode channel,

$$\Delta x = \frac{L}{J-1} \tag{26}$$

The step size Δt is chosen to be at least ten times smaller than the limit resulting from the Courant–Friedrichs–Lewy (CFL) stability condition [15] for the upwind scheme considered.

$$u\frac{\Delta t}{\Delta x} \leq 1 \tag{27}$$

The algebraic Eq. (24) can be manipulated to give a formula for the unknown values $y_i^{j,n+1}$, $i \in \{\mathrm{H_2}, \mathrm{N_2}\}$, in terms of the values at the nth time level, that is,

$$y_i^{j,n+1} = y_i^{j,n} + \left(\frac{u^{j-1,n} y_i^{j-1,n} - u^{j,n} y_i^{j,n}}{\Delta x} + \dot{y}_i^{j,n} \right) \Delta t \tag{28}$$

Note that the molar fraction of vapor is constant by assumption, and hence,

$$y^{j,n}_{\mathrm{H_2O}} = y_{\mathrm{H_2O}}, \quad \forall\, j,n \tag{29}$$

The velocity of the gas mixture at the nth time level can be calculated by rearranging Eq. (25).

$$u^{j-1,n} = \frac{1}{\Sigma_i y_i^{j-1,n}} \left(u^{j,n} \sum_i y_i^{j,n} - \Delta x \sum_i \dot{y}_i^{j,n} \right) \tag{30}$$

and since $y^{\mathrm{An}} = \Sigma_i y_i^{\mathrm{An}} = 1$ the following equation is obtained:

$$u^{j-1,n} = u^{j,n} - \Delta x \sum_i \dot{y}_i^{j,n} \tag{31}$$

The production/consumption rate of water vapor is determined from Eq. (19) as

$$\dot{y}^{j,n}_{\mathrm{H_2O}} = y^{\mathrm{An}}_{\mathrm{H_2O}} \frac{u^{j,n} - u^{j-1,n}}{\Delta x} \tag{32}$$

After some manipulations the combination of Eqs. (31) and (32) finally yields

$$u^{j-1,n} = u^{j,n} - \frac{\Delta x}{1 - y^{\mathrm{An}}_{\mathrm{H_2O}}} \cdot \sum_{i \in \{\mathrm{H_2}, \mathrm{N_2}\}} \dot{y}_i^{j,n} \tag{33}$$

The equations to compute the gas concentrations and the velocity profile along the anode channels (Eqs. (28) and (33)) still apply for systems where the number of channels decreases along the anode flow field as in PAC-Car II's case shown in Fig. 1. We approximate the complex anode flow field geometry with changes in the length and number of channels as shown in Fig. 5 and documented in Table 1. The change in channel number along the flow causes a discontinuous velocity profile after applying the boundary condition (23) at the position of the discontinuity in the channel number. Hence in our case, Eq. (33) is applied along the channel length starting with the velocity associated with the mass spectrometer flow rate up until the first switch from three to six

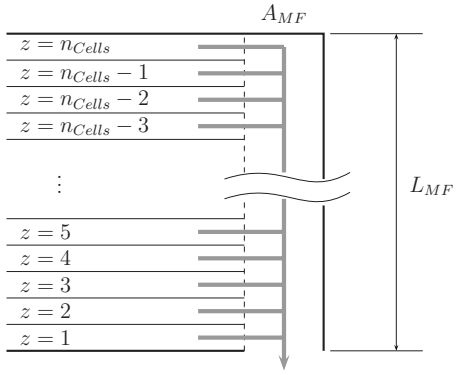

Fig. 6 Schematic of the connection between the anode channels and the anode outlet manifold

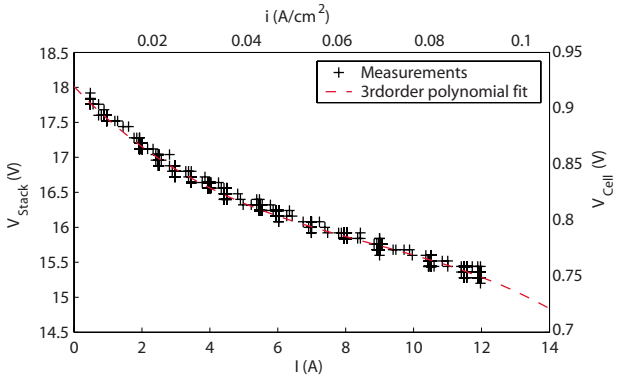

Fig. 7 Measured and fitted polarization curve of the PAC-Car II fuel cell stack

channels. At the channel number switch the flow speed is reduced by 50% and Eq. (33) is applied again until the next channel number switch.

3.6 Outlet Manifold Dynamics. The model equations so far yield the gas concentrations along the anode channels of the fuel cells. The individual anode mass streams are collected in a receiver, the anode outlet manifold, which is continuously sampled by the mass spectrometer. A schematic of the anode outlet manifold with cross-sectional area A_{MF} and length L_{MF} where the various fuel cells are connected is shown in Fig. 6.

A time delay has been considered for the calculation of the expected gas concentrations from the end of the anode channel to the end of the anode outlet manifold by assuming (i) uniform pressure and temperature conditions inside the outlet manifold, (ii) equal cell individual mass flow rates, and (iii) a constant cross-sectional outlet manifold area. The time delay is calculated assuming a linear velocity profile along the outlet manifold $dz/dt = u^* z$ with the flow speed increasing as it approaches the exit of the anode outlet with the exit flow speed matching the mass spectrometer flow $u^* L_{MF} = \dot{V}_{An}^{Out}/A_{MF}$. The time delay is, hence, determined as a function of the fuel cell position in the stack, $z \in \{1, \ldots, n_{Cells}\}$ and the outlet volumetric flow rate $\dot{V}_{An}^{Out}$, which is assumed constant, as

$$\Delta t_{MF}^{z} = \frac{A_{MF} L_{MF}}{\dot{V}_{An}^{Out}} \cdot \ln(z) \tag{34}$$

The resulting gas concentrations at the manifold outlet are then determined as the superposition of the individual cell concentrations, according to

$$y_i^{MFOut}(t) = \frac{1}{n_{Cells}} \cdot \sum_{z \in \{1,\ldots,n_{Cells}\}} y_i(L_{Ch}, t - \Delta t_{MF}^{z}) \tag{35}$$

3.7 Voltage Prediction. In order to estimate the impact of nitrogen accumulation on stack voltage, the polarization equation currently only considers the change in stack voltage as a function of the apparent current density $V_{Cell}(t) = V_{Cell}(i_{St}^{App}(t))$.

At low current densities, the cell overpotential depends on the gas crossover characteristics of the particular membrane electrode assembly. Hence, voltage measurements at low current densities (<0.1 A/cm^2) and two temperatures (50°C and 60°C) were collected and used to fit a third-order polynomial. The voltage values are recorded immediately following a purge when no water or nitrogen flooding effects are present. Data and polynomial approximation are shown in Fig. 7.

For higher current densities the cell ohmic resistance was chosen from Ref. [14]. The overall cell voltage (V_{Cell} in volts) as a function of current density (i in A/m^2) at 50°C and 60°C is calculated as

$$V_{Cell}^{50°C} = \begin{cases} \alpha_{V_4} + \alpha_{V_3} i + \alpha_{V_2} i^2 + \alpha_{V_1} i^3 & \text{for } i \le 10^3 \\ 0.7643 - 0.514 \times 10^{-4}(i - 10^3) & \text{for } i > 10^3 \end{cases} \tag{36a}$$

and

$$V_{Cell}^{60°C} = V_{Cell}^{50°C} - 0.019 \tag{36b}$$

with

$$\alpha_{V_4} = 0.9005$$
$$\alpha_{V_3} = -3.0578 \times 10^{-4}$$
$$\alpha_{V_2} = 3.1367 \times 10^{-7}$$
$$\alpha_{V_1} = -1.4406 \times 10^{-10} \tag{36c}$$

For this work, which only provides the proof-of-concept for the importance of the anode nitrogen buildup in the fuel cell performance, the polarization in Eqs. (36*a*)–(36*c*) has been calibrated for a limited set of conditions, i.e., specific anode and cathode pressures, stack temperatures, and humidification level. In future work the polarization equation will be extended for general operating conditions.

4 Simulations and Experimental Validation

Using the fuel cell stack parameters summarized in Table 1 and the permeability coefficients adopted from Ref. [7], the model is simulated using the numerical integration routines in the MATLAB computing software. The simulation results presented in Fig. 8(*a*) (for $t_{Sim} = 100$ s) and Fig. 8(*b*) (for $t_{Sim} = 2000$ s) were computed using the model described in Sec. 3 for the (constant) operating conditions summarized on the right top corner of each figure. The input variables of the model were chosen to approximate the conditions encountered in the experimental run shown in Fig. 2. Figure 8(*a*) shows an early snapshot (first 100 s) of the predicted spatially varying phenomena along the fuel cell channel, whereas Fig. 8(*b*) shows the predicted asymptotic (after 2000 s) spatial distributions.

The first subplot on the left side of both Figs. 8(*a*) and 8(*b*) shows the predicted velocity profile of the gas stream in the anode flow channels. Note the velocity discontinuity at the location that the channel number and area change. The second and third subplots on the left side of both Figs. 8(*a*) and 8(*b*) show the gas concentrations along the anode flow field. The diffusion rates of hydrogen and nitrogen are shown in the fourth subplot and the last subplot. On the right sides of Figs. 8(*a*) and 8(*b*), the gas concentrations at the system outlet (outlet of the anode channels, and

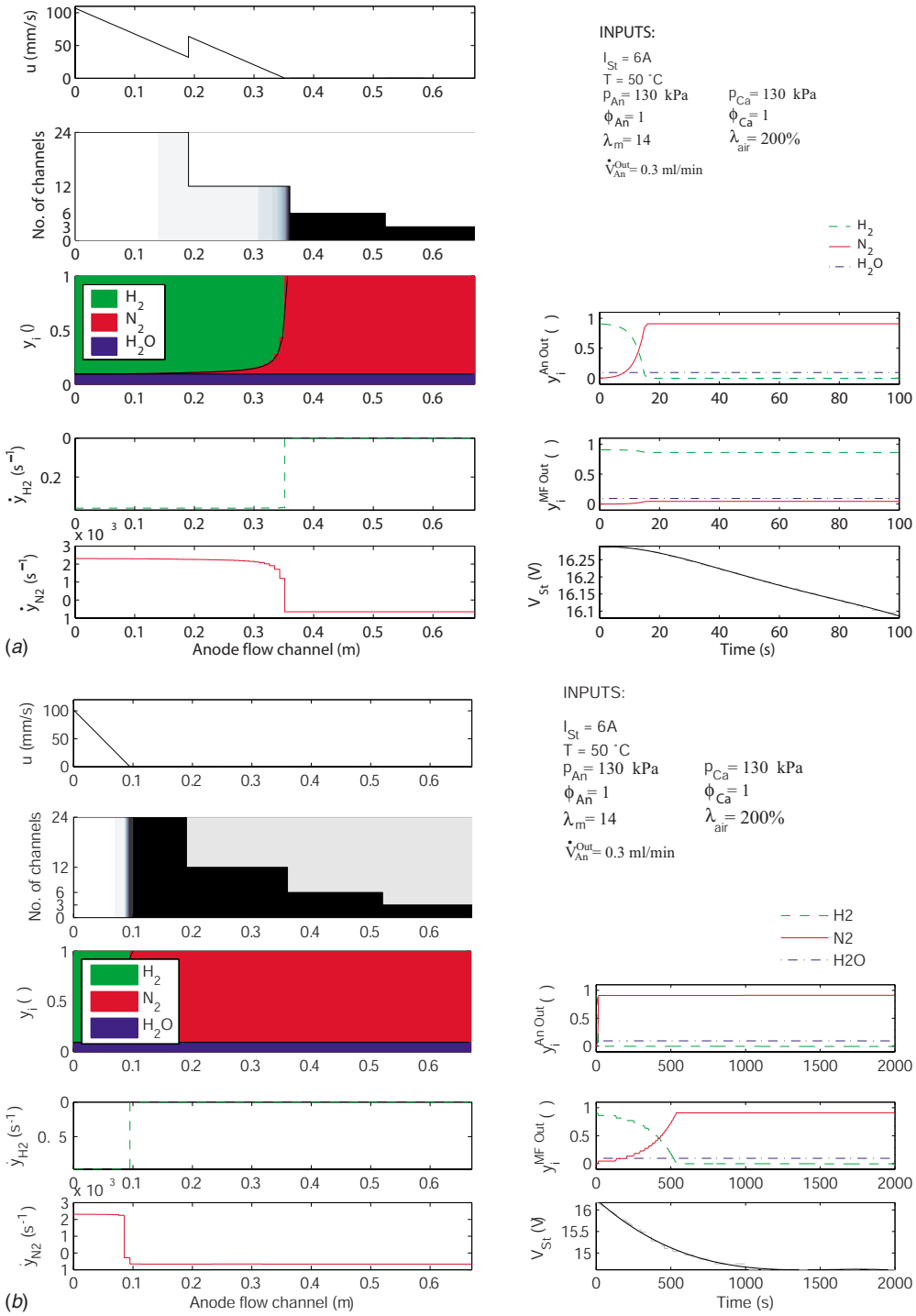

Fig. 8 Simulation results for (*a*) t_{Sim}=100 s and (*b*) t_{Sim}=2000 s

anode manifold outlet) and the stack voltage are shown after interpolation to smooth out the discontinuities arising through the discretization.

The left plots of Fig. 8(*a*) show that after 100 s approximately half of the fuel cell channel length has completely filled with stagnant nitrogen gas. At the areas with stagnant nitrogen, reaction of hydrogen is obviously suspended since there is no hydrogen to support the reaction. At the same areas, nitrogen is transferred from the anode to the cathode (bottom left plot) due to the concentration gradient across the membrane. Recall that the nitrogen concentration in the cathode is considered fixed and equal to the nitrogen concentration in the atmospheric air, namely, 75.3% by weight in the dry air. Figure 8(*b*) shows the asymptotic spatial distributions where more than 85% of the channel length is filled with nitrogen.

The first subplots to the right of Fig. 8(*a*) and 8(*b*) also show that it takes approximately 20 s before a steady state ($85\%N_2$, $0\%H_2$, $15\%H_2O$) concentration is reached in the flow out of the fuel cell channels, which indicates the time when the end of the channels start filling with nitrogen and consequently can cause hydrogen starvation and carbon corrosion [16]. The second subplots to the right of Fig. 8(*a*) and 8(*b*) show that it takes approximately 500 s before a steady concentration of $85\%N_2$ is

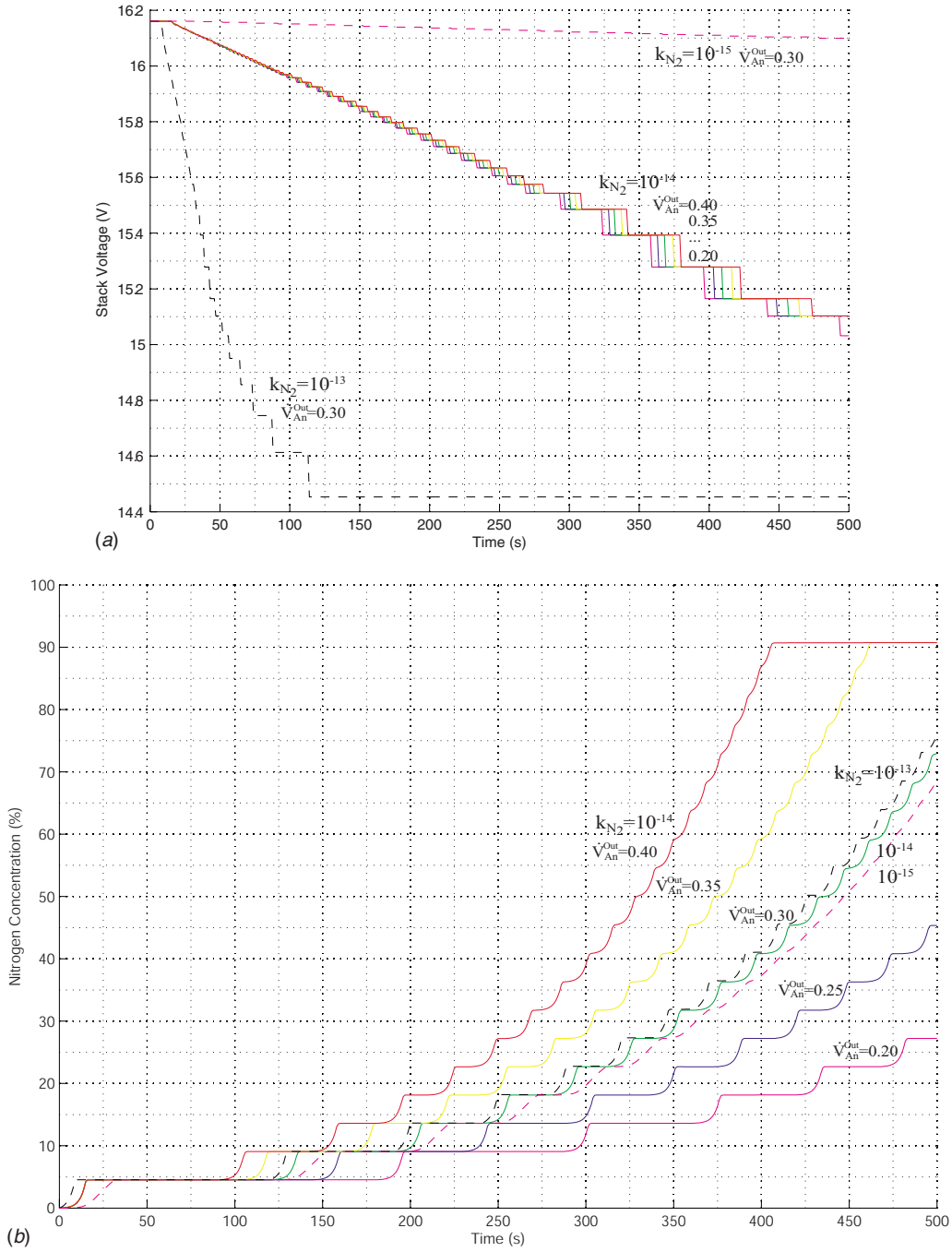

Fig. 9 Effects of k_{N_2} and $\dot{V}_{An}^{Out}$ variations on (*a*) voltage and (*b*) nitrogen for $I_{St}=6$ A, $T=50°C$, and $\lambda_{air}=200\%$

reached at the exit of the outlet anode manifold. The predicted voltage follows the temporal evolution of the stagnant N_2 front or the zero-velocity front and reaches steady state approximately after 1250 s, as shown in the last right subplot of Fig. 8(*b*).

For the simulations shown in Fig. 8 the flow out of the outlet manifold in Eqs. (23) and (34) was chosen as $\dot{V}_{An}^{Out}=0.3$ ml/min. This value was estimated through a series of separate experiments by measuring the pressure drop observed when the stack alone was pressurized and comparing it with the pressure drop when the pressurized stack was connected to the mass spectrometer. These leaklike tests were repeated with different H_2 and N_2 concentrations, namely, 50/50% or 0/100%. The corresponding estimated $\dot{V}_{An}^{Out}$ value varied pointing to a dependency of the mass spectrometer sample size on the actual concentration of the sample. Future work will focus on developing a testing process with a fixed volume sample to bypass the sensitivity of the standard mass spectrometer.

A sensitivity analysis was performed using numerical simulations of the model. The effects of two important model parameters, namely, the mass spectrometer flow $\dot{V}_{An}^{Out}$ and the nitrogen permeation coefficient k_{N_2}, are shown in Fig. 9. The upper subplot in Fig. 9(*a*) shows the $\dot{V}_{An}^{Out}$ value affects the prediction of nitrogen concentration. The lower subplot in Fig. 9(*b*), however, indicates that the variable $\dot{V}_{An}^{Out}$ does not affect the voltage prediction since the predicted voltage decrease depends on the predicted decrease

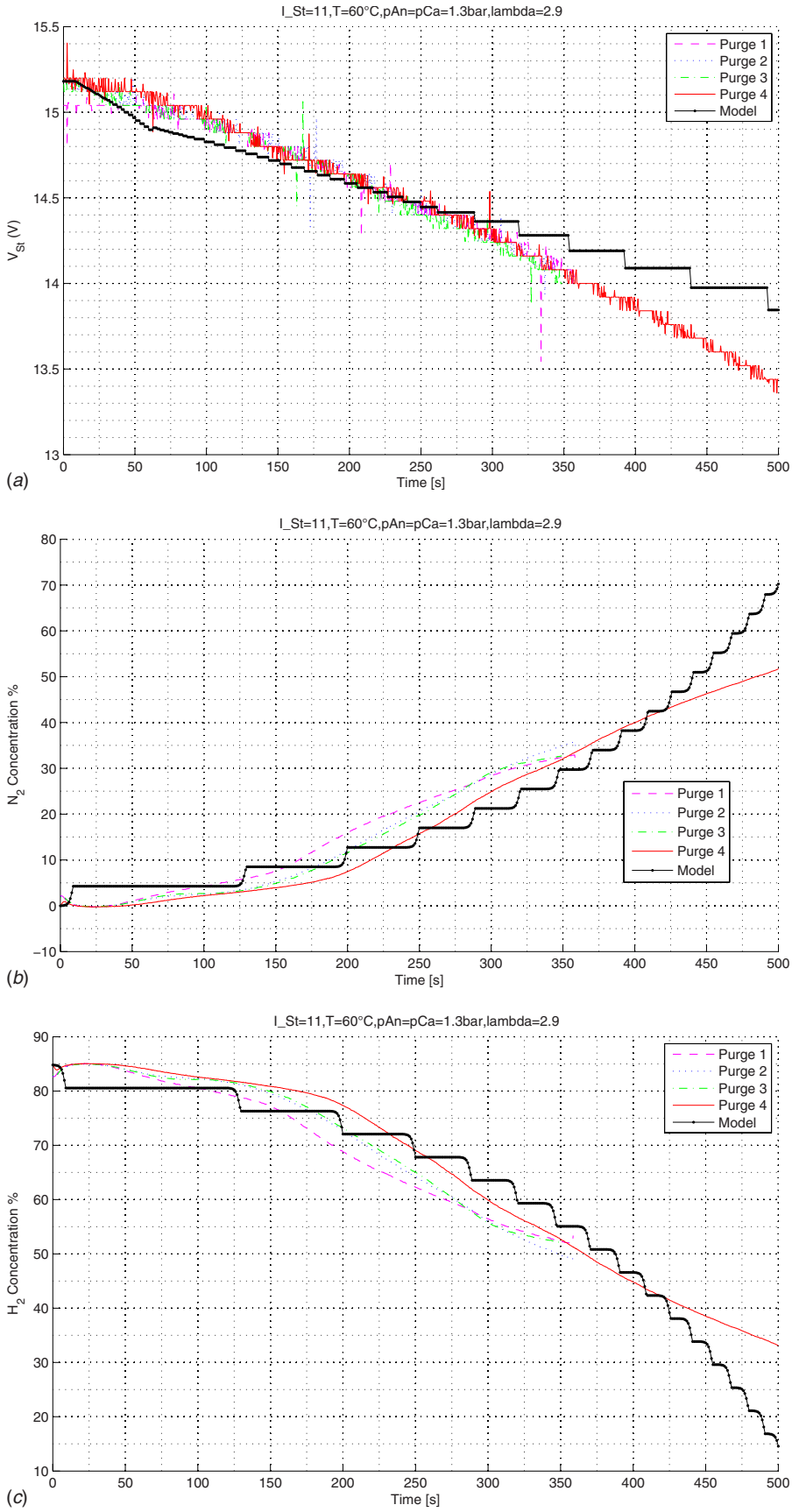

Fig. 10 Comparison between simulations for t_{Sim}=500 s and measurements for (a) stack voltage, (*b*) nitrogen concentration, and (*c*) hydrogen concentration

in the apparent active channel length calculated in Eq. (13), which is very sensitive on the consumption rate of hydrogen in Eq. (9) and the crossover of nitrogen in Eq. (17), and specifically the permeation coefficient of nitrogen k_{N_2}.

Note the different discrete changes in the voltage and the nitrogen concentration response. The differences are due to the fact that the two responses correspond to the two different dimensions of the 1+1 D model presented here, namely, the channel dimension and the outlet manifold dimension. Specifically, the voltage follows the concentration of hydrogen in the channels. Its drop corresponds to the change in current density, which follows the decrease in the discretized channel length as the zero-velocity front propagates up the channel length. The voltage decay slows down because the front moves slower and it crosses each channel discretization Δx slower. The opposite trend is observed in the simulation of the nitrogen concentration. The nitrogen builds up slower in the beginning and as time progresses the rate of nitrogen growth increases following the effects of the delay through the logarithm of the cell position (34) along the outlet manifold.

With constant model parameters, $\dot{V}_{An}^{Out}=0.3$ ml/min based on the leak-rate test measurements and $k_{N_2}=10^{-14}$ mol/m/s/Pa based on Ref. [7], the model predictions are compared with measurements in one more set of operating conditions, different from the ones shown or used so far. Figure 10 shows the model validation for when stack current is adjusted to $I_{St}=11$ A, the stack temperature is set to 60°C, and the cathode air supply $\lambda_{air}=290\%$ is 2.9 times larger than the air necessary for the stoichiometric reaction associated with the drawn current $I_{St}=11$ A. These new conditions mitigate the measurement problems associated with the accumulation of water in the anode, especially when a water droplet goes in the capillary of the mass spectrometer. An example of the measurement problems due to liquid water can be seen during the 2100–2200th second and after the 3900th second in the experiment shown in Fig. 2.

The validation plots show that the model predicts the overall nitrogen and hydrogen concentrations and the voltage decay during the first 6 min (360 s) of multiple purging periods. We postulate that some of the voltage mismatch observed in the very early phase (<70 s) arises from small diffusion of hydrogen from the outlet manifold to the anode channels. For the mismatch after 6 min, and especially, for the mismatch between the asymptotic predicted (converges after 1250 s or 21 min) and experimental (keeps on dropping after 21 min with the same decay rate) behavior of voltage, a quick investigation of the data suggests that large cell-to-cell variation could be the culprit. Specifically, the experimental data show that just before the sixth minute the cell-to-cell variation starts increasing beyond the typical 20 mV, deeming unpredictable conditions for the simple one-dimensional model presented so far. The measured gas concentrations agree well in shape and in magnitude with their estimated counterparts up until the nitrogen concentration exceeds 50% in the exit of the outlet manifold. The discrepancies between the predicted and measured concentrations after this point are most likely due to the decrease in volumetric flow $\dot{V}_{An}^{Out}$ of the mass spectrometer associated with the significant changes in the H_2 concentration in the exit flow.

5 Conclusions

The model predicts an accumulation of nitrogen in the anode channels of a fuel cell stack with high hydrogen utilization. This accumulation causes a reduction in the effective fuel cell active area, and, thus, results in a decay of stack voltage, which agrees with the measured voltage decay before significant cell-to-cell variations are observed in the experiment. In addition the measured gas concentrations agree reasonably well with their estimated counterparts up until the nitrogen concentration exceeds 50% in the exit of the outlet manifold.

The following points can be addressed to improve the prediction accuracy of the model:

(i) detailed parametrization of the voltage equation
(ii) validation of the assumption on convection dominant characteristics, especially at the end of the channels where the velocities are very small and diffusion might be important
(iii) modeling H_2O crossover and flooding similar to Ref. [17]
(iv) continuous estimation of the water content of the membrane
(v) calculation of the permeability coefficient for N_2 as a function of temperature and membrane humidity, $k_{N_2}=k_{N_2}(T,\lambda_m)$
(vi) modeling the gas losses due to leakage

On the experimental side, the sensitivity of the mass spectrometer flow on the concentration of the sample and the circular effect of the outlet flow on the fuel cell gas concentration suggest that a better measuring method is needed in this fuel cell application.

Concluding, the results presented in this work strongly indicate that accumulation of nitrogen in the anode channels is an important consideration because it is the cause of a significant decay of stack voltage. The relative significance between nitrogen buildup and water flooding of the anode channels will be carefully quantified in future work.

Acknowledgment

Financial support from U.S. National Science Foundation is gratefully acknowledged.

Appendix: Parameters of the System

In Table 1, the parameters of the fuel cell system are summarized. The geometrical parameters describe the geometry of the fuel cell stack used in the PAC-Car project. The permeability coefficients were adopted from Ref. [7].

References

[1] Chia, E.-S., Benziger, J. B., and Kevrekidis, I. G., 2006, "STR-PEM Fuel Cell as a Reactor Building Block," AIChE J., **52**(11), pp. 3902–3910.
[2] Woo, C., and Benziger, J. B., 2007, "PEM Fuel Cell Current Regulation by Fuel Feed Control," Chem. Eng. Sci., **62**, pp. 957–968.
[3] Knights, S. D., Colbow, K. M., St-Pierre, J., and Wilkinson, D. P., 2004, "Aging Mechanisms and Lifetime of PEFC and DMFC," J. Power Sources, **127**, pp. 127–134.
[4] Arcak, M., Görgün, H., Pedersen, L. M., and Varigonda, S., 2004, "An Adaptive Observer Design for Fuel Cell Hydrogen Estimation," IEEE Trans. Control Syst. Technol., **12**(11), pp. 101–110.
[5] Pukrushpan, J. T., Stefanopoulou, A. G., Varigonda, S., Pedersen, L. M., Ghosh, S., and Peng, H., 2005, "Control of Natural Gas Catalytic Partial Oxidation for Hydrogen Generation in Fuel Cell Applications," IEEE Trans. Control Syst. Technol., **13**(1), pp. 3–14.
[6] McKay, D. A., Ott, W. T., and Stefanopoulou, A., 2005, "Modeling, Parameter Identification, and Validation of Water Dynamics for a Fuel Cell Stack," ASME Paper No. IMECE2005-81484.
[7] Kocha, S. S., Yang, J. D. L., and Yi, J. S., 2006, "Characterization of Gas Crossover and Its Implications in PEM Fuel Cells," AIChE J., **52**, pp. 1916–1925.
[8] del Real, A., Arce, A., and Bordons, C., 2007, "Development and Experimental Validation of a PEM Fuel Cell Dynamic Model," J. Power Sources, **173**(1), pp. 310–324.
[9] Yi, J., and Nguyen, T., 1998, "An Along the Channel Model for Proton Exchange Membrane Fuel Cells," J. Electrochem. Soc., **145**(4), pp. 1149–1159.
[10] Pasaogullari, U., and Wang, C., 2005, "Two-Phase Modeling and Flooding Prediction of Polymer Electrolyte Fuel Cells," J. Electrochem. Soc., **152**(2), pp. A380–A390.
[11] Berg, P., Promislow, K., Pierre, J. S., Stumper, J., and Wetton, B., 2004, "Water Management in PEM Fuel Cells," J. Electrochem. Soc., **151**(3), pp. A341–A353.
[12] Berg, P., Caglar, A., St.-Pierre, J., Promislow, K., and Wetton, B., 2006, "Electrical Coupling in Proton Exchange Membrane Fuel Cell Stacks: Mathematical

and Computational Modelling," IMA J. Appl. Math., **71**, pp. 241–261.
[13] Santin, J., Onder, C., Bernard, J., Isler, D., Kobler, P., Kolb, F., Weidmann, N., and Guzzella, L., 2007, *The World's Most Fuel Efficient Vehicle: Design and Development of PAC-Car II*, vdf Hochschulverlag, Zurich, Switzerland.
[14] Santis, M., Schmid, D., Ruge, M., Freunberger, S., and Büchi, F., 2004, "Modular Stack-Internal Air Humidification Concept-Verification in an 1 kW Stack," Fuel Cells, **4**, pp. 214–218.
[15] Fletcher, C. A. J., 2000, *Computational Techniques for Fluid Dynamics*, 2nd ed., Springer, Berlin.
[16] Meyers, J. P., and Darling, R. M., 2006, "Model of Carbon Corrosion in PEM Fuel Cells," J. Electrochem. Soc., **153**(8), pp. A1432–A1442.
[17] McKay, D. A., Siegel, J. B., Ott, W., and Stefanopoulou, A. G., 2008, "Parameterization and Prediction of Temporal Fuel Cell Voltage Behavior During Flooding and Drying Conditions," J. Power Sources, **178**(1), pp. 207–222.